Negative-ion formation by H^0/H^- projectiles grazing scattering from the MgO(100) surface

Guangyi Wang,[1] Hu Zhou,[2,*] Zewen Zong,[3] and Ximeng Chen[3]
[1]*School of Electronic and Information Engineering, Lanzhou City University, Lanzhou 730000, China*
[2]*School of Science, Xi'an Polytechnic University, Xi'an 710048, China*
[3]*School of Nuclear Science and Technology, Lanzhou University, Lanzhou 730000, China*

(Received 3 June 2021; accepted 1 October 2021; published 22 October 2021)

A simple theoretical model used to treat the formation of negative ions during H^-/H^0 grazing scattering from the MgO(100) surface is presented. It is revealed that the resonant transfer from projectiles to the conduction band and the detachment of tunneling Coulomb repulsive barrier to the vacuum of the affinity electron of H^- ions both play an important role in the electron-loss processes. The negative-ion destruction is dominated by a nearly resonant electron loss in the low projectile energy region of $E \leqslant 0.7$ keV (velocities $v \leqslant 0.17$ a. u.), whereas the detachment by Coulomb repulsive barrier tunneling during the interaction between projectiles and surface anion sites becomes efficient in the high-energy region of $E \geqslant 1.2$ keV ($v \geqslant 0.22$ a. u). Combined with the valence-band electron capture, our present calculation results of the negative ion yields are in good agreement with the available experimental data in the whole velocity region.

DOI: 10.1103/PhysRevA.104.042815

I. INTRODUCTION

Dielectric surfaces have considerable technical and enlightening significance, especially insulating ionic crystals, such as oxides, alkali-metal halides, etc., which have a large number of industrial applications in catalysis, microelectronics, gas sensors, etc. [1], most of which employ chemical reactions and adsorption on surfaces usually involving electron transfer processes [2]. Therefore, numerous experiments and theories of various projectile–ionic crystal target combinations were carried out on charge exchange, electron emission, secondary ion emission, implantation [3,4], and image charge phenomena [5–17]. In particular, the evolution of the charge states of atom or ion projectiles in low-energy (several keV to tens of keV), grazing incidence ($\varphi \approx 0.5^\circ$–$5^\circ$) collisions has been studied, and a very large negative ion yield is recorded using neutral projectiles [8,9], despite the large energy difference between occupied valence-band states and the affinity levels of the gas phase negative ions. This negative-ion formation of grazing scattering from surfaces of ionic crystals could be efficiently used for production of negative-ion beams, which is very attractive, for instance, to the design of negative-ion beam sources [6], neutral particle detectors in space research [18], facilitating nerve tissue growth [19], laser cooling of negative ions [20–22], probe for the subband electronic structures of nanosurfaces [23], and astrophysics evolution [24].

With projectile-insulator systems, ionic crystals of alkali-metal halide such as LiF, KI, and KCl have been studied in depth both experimentally and theoretically [8,12]. For the very important case of oxide surfaces, such studies are relatively few and only on MgO. In experiments with a MgO(100) surface, the formation of a very high negative ion fraction (H^-, O^-, and F^- are 7%, 35%, and 75%, respectively [9]) from neutral atoms has been observed in the incident energy range from a few hundred eV to a few keV, and the existence of electron-loss processes has been proved. That is, there are two kinds of electron transfer of atom or ion grazing scattering from MgO surfaces: the formation and destruction of negative ions [9–11]. Significantly different from F projectiles, the disappeared "memory" of the initial charge states of both H^0 and H^- projectiles demonstrates the existence of different electron-loss channels in the same experiment [9]. Therefore, multiple electron-loss channels of hydrogen negative ions in front of the MgO(100) surface are significant.

From a practical perspective, hydrogen beam injection into plasma fusion devices is very exciting [25]. Hence it is important to understand such charge transfer on a more fundamental level in the behavior of the H^- negative ion yield, as well as chemical reactions and adsorption. The electron-capture mechanism of neutral atom grazing scattering from oxides surfaces, similar to the case of alkali-metal halide surfaces, has been properly understood. Negative ions are formed via a binary type collision of the neutral projectiles with the negatively charged lattice ions [10]. For the destruction of negative ions, several different mechanisms have been proposed, but their relative efficiency is still unresolved [12]. Deutscher *et al.* [11] made an assumption of a constant destruction probability of 98.3% to reproduce the experimental negative ion yield. For the multiple electron-loss channels of hydrogen negative ions in front of a MgO(100) surface, the electron detachment of tunneling the Coulomb repulsive barrier to the vacuum [13,14] in the encounter of negative projectiles with the negatively charged lattice ions should be one of them. In addition, due to the confluence of the affinity level of a H^- ion and the conduction-band energy level of a MgO crystal [10], clearly one can expect that the electron loss to the unoccupied

*zhouhu19860224@163.com

 ©2021 American Physical Society

conduction-band states via a nearly resonant electron transfer may participate in the destruction of negative ions.

In this work, a simple theoretical model used to treat the destruction of negative ions during H^-/H^0 grazing scattering from the MgO(100) surface is presented. For the negative-ion destruction, one can find that the nearly resonant transfer from projectiles to the conduction band takes a major part only in the low projectile energy region, $E \leqslant 0.7$ keV [velocities $v \leqslant 0.17$ a.u. (note that throughout this paper, "a.u." means "atomic units")], whereas the detachment by Coulomb repulsive barrier tunneling during the interaction between projectiles and surface anion sites becomes efficient in the high-energy region $E \geqslant 1.2$ keV ($v \geqslant 0.22$ a.u.). Combined with the valence-band electron capture, we have obtained a good reproduction of the available experimental data using the present model in the whole energy region.

The paper is organized as follows: Section II briefly reviews the theory of the binary collision model. Section III deals with the description of computational details of the energy defect (the energy difference between the initial and the final states), and finally Sec. IV presents the electron-capture and -loss mechanisms, as well as the comparison between our present results of the theoretical calculation and the available experimental data. Atomic units are used unless otherwise stated.

II. THEORY

Similar to alkali-metal halides, MgO is a predominantly ionic crystal, consisting of ions of alternate charge, with a structure similar to the LiF crystal, having a lattice constant of $a = 7.9554$ a.u. [26,27]. At the same time, the band structure of MgO is similar to that of the alkali-metal halides with the band gap width of $E_g \approx 7.8$ eV [28,29]. The valence-band electrons of MgO crystal are localized at the oxygen anion sites [10], and the conduction band mainly originates from the Mg($3s$) orbitals [9]. With minor modifications resulting from the Mg^{2+} and O^{2-} charges of the ions at lattice sites, these similarities make the method put forward in Ref. [14] also applicable to the studied MgO target here.

A. Binary collision model of electron capture

After an electron was captured by a neutral $P^0_{\rm gas}$ projectile from the valence band near a $O^{2-}_{\rm as}$ anion site of the MgO(100) surface, a corresponding hole was left at this anion site. On the timescale of the interaction between the projectile and the $O^{2-}_{\rm as}$ site, the diffusion of this hole is negligible [27]. However, when the formed negative ion moved to other lattice sites, the produced hole was filled by other valence-band electrons and diffused to other anion sites. Therefore, the electron-capture process can be regarded as a neutral projectile $P^0_{\rm gas}$ undergoing a series of sequent binary collisions with doubly charged oxygen lattice sites, $O^{2-}_{\rm as}$ [15,16],

$$P^0_{\rm gas} + O^{2-}_{\rm as} \rightarrow P^-_{\rm gas} + O^-_{\rm as}. \tag{1}$$

The binary collision event of Eq. (1) is schematically shown in Fig. 1. The "active site" indicated as $O^{2-}_{\rm as}$ is placed at the origin of the frame of coordinate system XYZ, and the projectile is located at $\mathbf{R}$. Other lattice sites of the crystal are

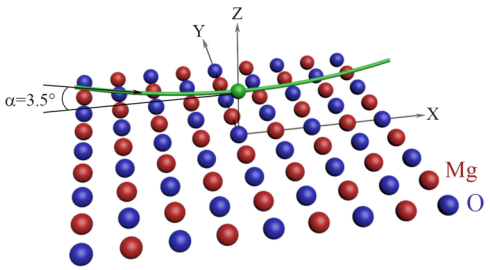

FIG. 1. Sketch of the H^0−MgO(100) collision system. Only surface sites of the MgO ionic crystal are displayed. The MgO ionic crystal consists of alternating point charges, corresponding to Mg and O lattice sites, respectively. $\alpha = 3.5^\circ$ represents the incident angle of projectiles.

viewed as spectators and point charges (PCs) for simplicity. The computation essentially follows the method reported in Refs. [15,16], so only a brief overview is given below.

A key of electron transfer process is the "energy defect," that is, the difference between the energies of the initial and final states,

$$\Delta E_{\rm cap}(\mathbf{R}, v) = E(P^-_{\rm gas} + O^-_{\rm as}) - E\left(P^0_{\rm gas} + O^{2-}_{\rm as}\right). \tag{2}$$

As in Ref. [30], considering both ML (Mott-Littleton) polarization $P_{\rm ML}(\mathbf{R})$ and image interaction $U_{\rm image}(\mathbf{R}, v)$ contributions in the final state of the electron-capture reaction of Eq. (2), the energy defect can be rewritten as

$$\Delta E_{\rm cap}(\mathbf{R}, v) = \varepsilon_{O^{2-}_{\rm as}} - \varepsilon_{P^-_{\rm gas}} + \sum_{\mathbf{r}_i \neq 0} \frac{q_i}{|\mathbf{r}_i|} + V_{\rm Mad}(\mathbf{R}) + P_{\rm ML}(\mathbf{R}) + U_{\rm image}(\mathbf{R}, v), \tag{3}$$

where $\varepsilon_{O^{2-}_{\rm as}} = E_{O^-_{\rm as}} - E_{O^{2-}_{\rm as}}$ and $\varepsilon_{P^-_{\rm gas}} = E_{P^0_{\rm gas}} - E_{P^-_{\rm gas}}$ give the binding energies of electrons for free O^{2-} ion and free $P^-_{\rm gas}$, respectively. $V_{\rm Mad}(\mathbf{R}) = \sum_i \frac{Qq_i}{|\mathbf{R}-\mathbf{r}_i|} + \frac{Q}{\mathbf{R}}$ is the Madelung potential experienced by the projectile of charge $Q = -1$ with the MgO ionic crystal (detailed description seen in Ref. [10]). $V_{\rm Mad}(\mathbf{R})$ is mainly determined by the second attractive term, which represents the interaction between the projectile of charge -1 and the hole of charge $+1$ at the active site after a valence-band electron was removed. The summation of the third term runs with the exception of the active site over all i lattice sites with charge q_i of approximately infinite crystals.

B. Binary collision model of electron loss

Since the conduction-band electrons of MgO are localized at Mg cation sites, the loss of the affinity electron of a negatively charged projectile to the conduction band [corresponds to Mg($3s$) orbitals] can be also treated by a binary type collision of the projectile with a doubly charged Mg "active site." As for projectiles with negative charge $Q = -1$ encountering a Mg^{2+} cation at the surface, the electron-loss process can be regarded as

$$P^-_{\rm gas} + Mg^{2+}_{\rm as} \rightarrow P^0_{\rm gas} + Mg^+_{\rm as}. \tag{4}$$

Similar to the electron-capture model, the energy defect that determines the efficiency of the electron loss is given by

$$\Delta E_{\rm LS}(\mathbf{R}, v) = \varepsilon_{P^-_{\rm gas}} - \varepsilon_{\rm Mg^{1+}_{as}} + \sum_{i\neq k} \frac{(-1)q_i}{|\mathbf{r}_i - \mathbf{r}_k|} - \sum_i \frac{Qq_i}{|\mathbf{R} - \mathbf{r}_i|} - U_{\rm image}(\mathbf{R}, v). \quad (5)$$

In Eq. (5), $\varepsilon_{\rm Mg^{1+}_{as}} = E_{\rm Mg^{2+}_{as}} - E_{\rm Mg^{1+}_{as}}$ is the binding energy of an electron for a free Mg^{1+} ion. It should be noted here that there is no ML-polarization interaction contribution to the energy defect of the electron-loss process. The Mg "active site" is located at $\mathbf{r}_k$ and the summation runs over all i lattice sites ($\mathbf{r}_i$) except the active site ($\mathbf{r}_k$) in the third term, which is the interaction energy between the electron left at the Mg active site and all point charges of other sites of the crystal. Finally, the fourth term is electrostatic interaction between the negatively charged projectile and the neutral MgO crystal in the initial state.

III. COMPUTATIONAL DETAILS OF THE ENERGY DEFECT

A. Ionic charges and potential of the MgO crystal

For simplicity the projectiles and all lattice sites of the MgO ionic crystal are treated as PCs. The "active site" at the ionic crystal surface that participates in a binary type charge transfer is also treated as a PC [10,15,16]. For the nonactive sites of a MgO crystal, the charge of ±2 has been shown to give correct results in quantum chemistry studies [31,32], while somewhat different charges (close to unity) have also been used in several model chemisorption calculations [33–36]. It should be noted here that due to a higher Madelung potential obtained by PCs of charge ±2, in some typical calculations of the Madelung potential of a MgO crystal, the absolute value of charges of MgO lattice ions is usually fixed to be less than 2 [35].

In our present model, the ionic charges of the bulk and (100) surface of MgO in Ref. [33] are employed, that is, ±1.14 for the (100) surface and ±1.12 for bulk. Employing these fixed ionic charges, the interaction energy between the O anion site and all other lattice sites is −12.591 eV. Also, since the binding energies of the valence-band electrons can be well approximated by the affinity of the free O^{2-} ($\varepsilon = 0$ eV because of the nonexistence of free O^{2-} ions [10]) shifted by the Madelung potential of the rest of the lattice ions in the crystal (other effects can be neglected [12]), the binding energies of the valence-band electrons obtained by our present model are in close agreement with the value of −11.5 eV obtained from experiment [29]. Thus, the values of the ionic charges used here are plausible.

Furthermore, based on the above discussion, we can replace $\varepsilon_{\rm O^{2-}_{as}} + \sum_{\mathbf{r}_i\neq 0} \frac{q_i}{|\mathbf{r}_i|}$ by $E_{\rm VB} = -11.5$ eV [29] (the mean binding energy of valence-band electrons) in Eq. (3), and the energy defect of valence-band electron capture of Eq. (3) can be expressed as

$$\Delta E_{\rm cap}(\mathbf{R}, v) = E_{\rm VB} - \varepsilon_{P^-_{\rm gas}} + V_{\rm Mad}(\mathbf{R}) + P_{\rm ML}(\mathbf{R}) + U_{\rm image}(\mathbf{R}, v). \quad (6)$$

Similarly, $\varepsilon_{\rm Mg^{1+}_{as}} + \sum_{i\neq k} \frac{q_i}{|\mathbf{r}_i - \mathbf{r}_k|}$ can be replaced by $E_{\rm CB} = -1.3$eV [29] (the binding energy of the bottom of the conduction band) in Eq. (5). Hence, the energy defect of electron loss to the conduction band can be rewritten as

$$\Delta E_{\rm LS}(\mathbf{R}, v) = \varepsilon_{P^-_{\rm gas}} - E_{\rm CB} - \sum_i \frac{Qq_i}{|\mathbf{R} - \mathbf{r}_i|} - U_{\rm image}(\mathbf{R}, v). \quad (7)$$

B. Effective area

A three-dimensional grid of 2205 lattice ions arranged in five parallel layers with a lattice constant of $a = 7.9554$ a.u. was used to model the surface of the MgO(100). Similar to the treatment in Refs. [13,14], the lattice ions were viewed as PCs; this guarantees the accuracy of the calculated Madelung potential at the surface anion site to be greater than 5×10^{-4} eV. Considering the scales of projectile interacting with the surface,$O^{2-}_{\rm as}$, and the projectiles' trajectories passing over the area above the $O^{2-}_{\rm as}$ along different directions, the effective area of $O^{2-}_{\rm as}$ taken to be the origin of the (X,Y,Z) coordinate is $S = \{-\frac{a}{4} \leqslant X \leqslant \frac{a}{4},\ -\frac{a}{4} \leqslant Y \leqslant \frac{a}{4}\}$. The final transition probability $P^{\rm site}(Z)$ in one single binary collision with an $O^{2-}_{\rm as}$ can be obtained by averaging $P(S, Z)$ over trajectories in S. $P^{\rm site}(Z)$ gives the probability of electron transfer of a projectile lying in an (XY) plane which is parallel to the (100) surface and at altitude Z above the $O^{2-}_{\rm as}$. Thus the energy defect that determines the electron transfer probability could be obtained by averaging $\Delta E(\mathbf{R}, v)$ over S, $\langle \Delta E(\mathbf{R})\rangle_S = \frac{1}{S}\iint_S \Delta E(X, Y, Z)dXdY$. The same as in Ref. [15], if the projectile velocity v is given, $\langle \Delta E\rangle_S$ is only a function of surface altitude Z.

C. ML polarization and image interaction effects

The correction terms of ML polarization and image interaction effects to the energy defect have been discussed in detail in Refs. [14,37]. Upon an electron capture, a hole created at the active site of the previous neutral crystal is equivalent to a charge of +1. The projectile of charge −1 and the hole result in an electric dipole moment, whose field polarizes lattice ions. Thus, an additional field-induced dipole ("Mott-Littleton interaction" [30]) contributes to the energy of the final state. Clearly, the image interaction [38,39] between the negatively charged projectile and its own image charge created by the polarization of crystal also introduces a correction to the energy of the final state. The related computational parameters were taken from Refs. [40,41], respectively, for the ML polarization and the image interaction. The calculated results of these two corrections are both shown in Fig. 2. For the ML polarization effect [see Fig. 2(a)], the average result $\langle P_{\rm ML}(X, Y, Z)\rangle_S$ for a surface altitude range of $Z \in [2.5, 5]$a.u. is presented. For the image interaction [see Fig. 2(b)], the results for the fixed altitude, respectively, at 2.5, 3.0, 3.5, 4.0, and 5.0 a.u. and $\langle P_{\rm ML}(X, Y, Z)\rangle_S$ averaged over an altitude range of $Z \in [2.0, 5.0]$ a.u. are given.

IV. RESULTS AND DISCUSSION

A. Electron capture

The energy defect between initial and final states plays a key role in the determination of any charge transfer process.

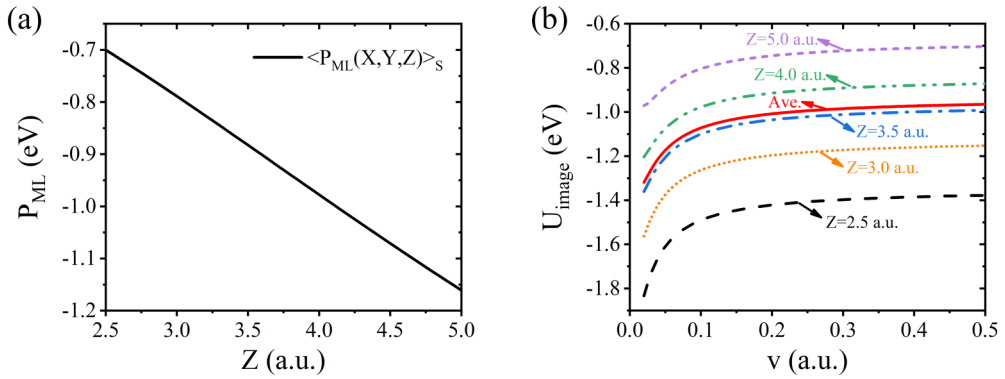

FIG. 2. (a) The result of ML polarization interaction $P_{\mathrm{ML}}(\mathbf{R})$ averaged over the effective area S of a surface O_{as}^{2-}, $\langle P_{\mathrm{ML}}(X,Y,Z)\rangle_S$ within surface altitude range of $Z \in [2.5, 5.0]$ a.u. (b) The results of image interaction $U_{\mathrm{image}}(Z, v_\parallel)$ for fixed Z, respectively, at 2.5, 3.0, 3.5, 4.0, and 5.0 a.u., and the averaged $U_{\mathrm{image}}(Z, v_\parallel)$ over the surface altitude range of $Z \in [2.5, 5.0]$ a.u.

According to Eq. (6) and results of the corresponding ML polarization and image interaction presented in the previous section, one can obtain the energy defect of valence-band electron capture by a projectile. As displayed in Fig. 3(a), the main behavior of valence-band electron-capture energy defect $\Delta E_{\mathrm{cap}}(Z, v)$ is determined by surface altitude Z. The dependence of $\Delta E_{\mathrm{cap}}(Z, v)$ on velocity v here results from a slight increase in v of the image interaction, $U_{\mathrm{image}}(Z, v_\parallel)$. Figure 3(b) presents the $\Delta E_{\mathrm{cap}}(Z, v)$ projections on velocity v for the fixed altitude, respectively, at $Z =$ 2.5, 3.0, 3.5, 4.0, and 5.0 a.u. and the average result of $\langle \Delta E_{\mathrm{cap}}(Z, v)\rangle_{Z\in[2.5,5.0]\mathrm{a.u.}}$. Clearly, the electron-capture process proceeds with a finite energy defect. Therefore, similar to the description in Refs. [5,12–14,17], one can estimate the probability of valence-band electron capture in a binary collision of a projectile with a surface O_{as}^{2-} by the nonresonant charge transfer model of Demkov [42] as follows:

$$P_{\mathrm{cap}}(\Delta E, v) = \frac{1}{2}\mathrm{sech}^2\left[\frac{\pi(\Delta E + v^2/2)}{2\gamma v}\right], \tag{8}$$

where γ characterizes the exponential decay of electron transfer interaction $V = V_0 \exp(-\gamma R)$, estimated from $\gamma = (\sqrt{2\varepsilon_{O^{2-}_{\mathrm{active}}}} + \sqrt{2\varepsilon_{H^-_{\mathrm{gas}}}})/2$ [12].

B. Conduction-band electron loss

As discussed above, only states close to the bottom of the conduction band can participate in the destruction of negative ions via a nearly resonant charge transfer. This point is fulfilled by the energy defect (as shown in Fig. 4) of resonant electron loss in the H^-−MgO(100) collision system. The energy defect $\Delta E_{\mathrm{LS}}(\mathbf{R}, v)$ was calculated by Eq. (7) and the three-dimensional (3D) plot of $\Delta E_{\mathrm{LS}}(Z, v) = \langle \Delta E_{\mathrm{LS}}(\mathbf{R}, v)\rangle_S$ is shown in Fig. 4(a). For clearly seeing the altitude dependence of the energy defect, the results of $\Delta E_{\mathrm{LS}}(Z, v)$ projections on velocity v for fixed Z, respectively, at $Z = 2.5, 3.0, 3.5, 4.0$, and 5.0 a.u. are shown in Fig. 4(b). It can be seen that the magnitude of the energy defect at $Z > 3$ a.u. is less than 1 eV and the average result, $\langle \Delta E_{\mathrm{LS}}(Z, v)\rangle_{Z\in[2.5,5.0]\mathrm{a.u.}}$, is within a range of $\langle \Delta E_{\mathrm{LS}}\rangle_{Z\in[2.5,5.0]\mathrm{a.u.}} \in [0.25, 0.65]$ eV. As expected, the sub-eV energy defect leads to the electron loss to the unoccupied states of the conduction band via a nearly resonant charge transfer process.

The probability of the electron loss to the conduction-band states, P_{LS}, can be simply expressed as [43]

$$P_{\mathrm{LS}}(v) = 1 - \exp\left(\frac{-\beta}{v_\parallel}\right), \tag{9}$$

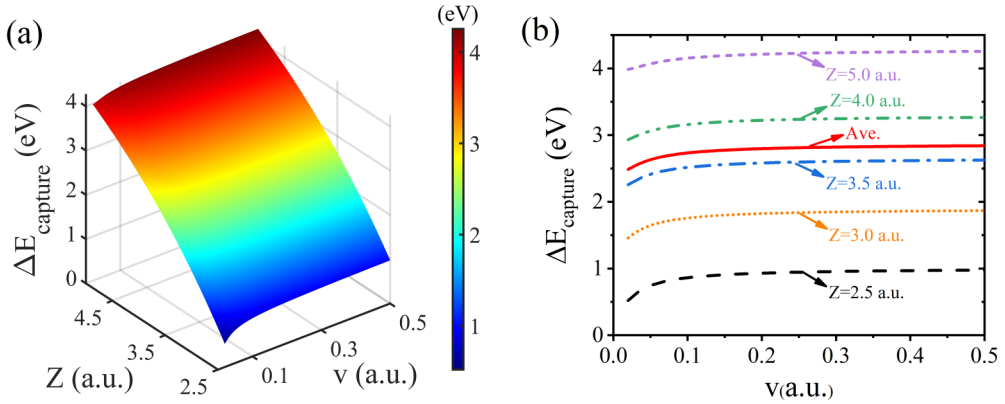

FIG. 3. (a) The 3D plot of the electron-capture energy defect $\Delta E_{\mathrm{cap}}(Z, v)$ as a function of projectile surface altitude Z and velocity v. (b) The projections on v for fixed Z at 2.5, 3.0, 3.5, 4.0, and 5.0 a.u., respectively. The solid line represents the result of ΔE_{cap} averaged over the Z range of $Z \in [2.5, 5.0]$ a.u..

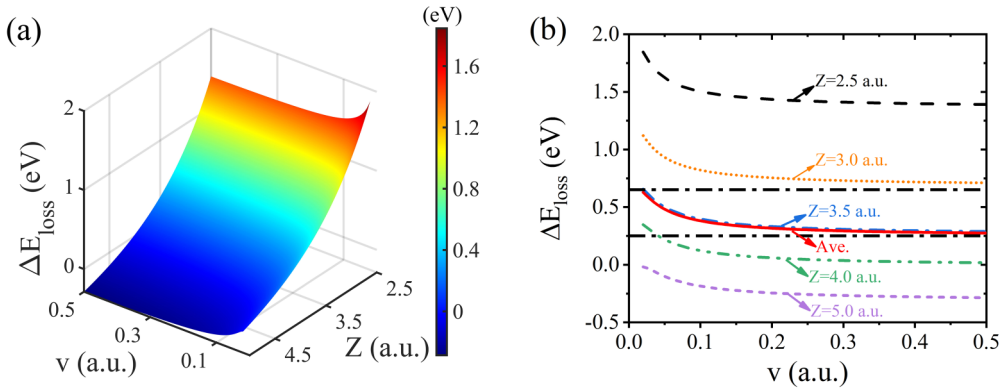

FIG. 4. (a) The 3D plot of the electron-loss energy defect $\Delta E_{\rm LS}(Z, v)$ as a function of projectile surface altitude Z and velocity v. (b) The projections on v for fixed Z at 2.5, 3.0, 3.5, 4.0, and 5.0 a.u., respectively (dotted lines). The solid line is the average result, $\langle \Delta E_{\rm LS}(Z, v)\rangle_{Z\in[2.5,5.0]\text{a.u.}}$. The black dotted parallel lines denote the constant energy defects of $\Delta E_{\rm LS}(Z, v) = 0.25$ and 0.65 eV.

where $v_\parallel = v\cos\alpha(\alpha = 3.5^\circ)$ is the velocity component parallel to surface. The parameter β closely relates to the electron-loss coupling strength between a H^- projectile and the unoccupied conduction-band states. An accurate estimate to the coupling strength requires a complicated quantum chemical calculation and is not the main scope of our present work. Here, the comparison of the calculated negative ion yields by taking $\beta = 0.1$, 0.2, and 0.3, respectively, and the available experimental data implies that within the uncertainty of experimental measurement the β values taken from $\beta \in [0.1, 0.3]$ are all acceptable [seen in Fig. 6(a) of Sec. IV D].

C. Quantum tunneling detachment

As reported in Refs. [13,44], a short-range binary encounter of a negative ion with a surface anion site causes the detachment of its affinity electron into vacuum. Therefore, one can expect the detachment of the affinity electron of a H^- projectile by the Coulomb repulsive barrier tunneled to

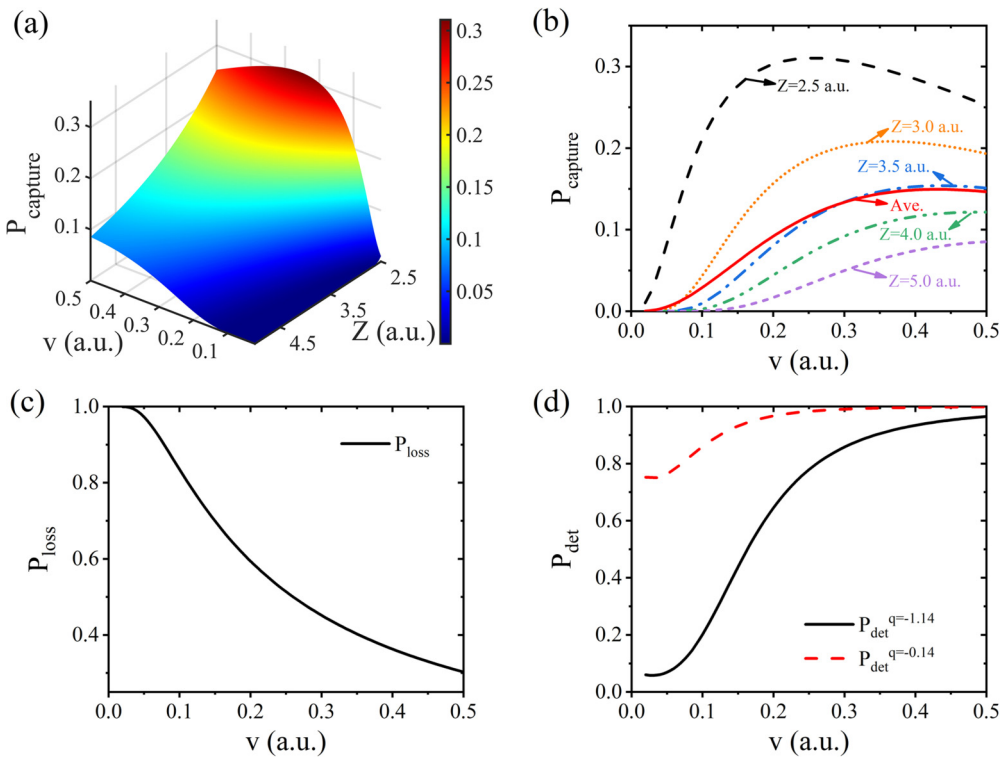

FIG. 5. (a) The 3D plot of the electron-capture probability $P_{\rm cap}(Z, v)$ as a function of projectile surface altitude Z and velocity v. (b) The projections on v for fixed Z, respectively, at 2.5, 3.0, 3.5, 4.0, and 5.0 a.u. (dotted line) and the average result, $\langle P_{\rm cap}(Z, v)\rangle_{Z\in[2.5,5.0]\text{a.u.}}$ (the solid line). (c) The probability of electron loss to the conduction band. (d) The detachment probabilities of the affinity electron of a H^- ion interacting with surface $O_{\rm as}^{q_{\rm eff}}$ of effective charge $q_{\rm eff} = -1.14$ (solid line) and $q'_{\rm eff} = -0.14$ (dashed line), respectively.

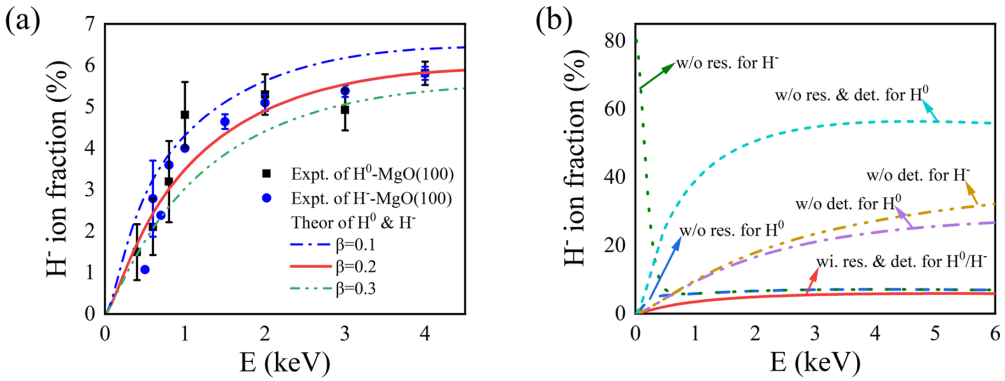

FIG. 6. (a) Total negative ion fractions as a function of incident energy E. Symbols represent the available experimental data from Ref. [9]. The lines represent the theoretical calculation results of negative ion fractions for H^- and H^0 incidence with β values, respectively, at $\beta = 0.1$ (blue dashed-dotted line), 0.2 (red solid line), and 0.3 (green dashed-dot-dotted line). (b) Total negative ion yields for $H^-/H^0 - MgO(100)$ collision systems obtained, respectively, without including quantum tunneling detachment (det.) and resonant electron loss (res.). The red solid line represents the result obtained with including all the negative-ion destruction channels.

vacuum level during the interaction with a surface O^{2-}_{site} of the MgO crystal. The detailed computations follow essentially the method reported in Refs. [13,14], so only a brief outline is given here. The detachment probability of the affinity electron of a negative projectile can be expressed by

$$P_{det}(E_\perp) = \exp[-2\Gamma(E_\perp)]. \tag{10}$$

Using the same treatment as in Ref. [17], $E_\perp = E'_\perp - U_{image}(Z, v)$ here is the corrected energy of the effective projectile electron, in which $E'_\perp = M(v \sin\alpha)^2/2$ is the vertical component of projectile energy, M is the atomic mass of the projectile, and α is the projectile incident angle with respect to the surface plane. The correction of $U_{image}(Z, v)$ to the effective projectile electron energy here originates from the image attraction between a H^- projectile and the image charge that is induced on the MgO(100) surface. This term increases the vertical energy component $E'_\perp$ for the motion along the surface normal. The decay rate Γ is given by

$$\Gamma(E_\perp) = \int_{r_1}^{r_2} \sqrt{2(V(r) - E_\perp)}dr, \tag{11}$$

where $V(r) = q_{eff}/r$ is the Coulomb potential created by the effective charge of the surface lattice anion participating in the Coulomb tunneling detachment process. The upper and lower limits of the integration are, respectively, the outer turning point r_2 where the orbit becomes classically allowed [$r_2 = q_{eff}/E_\perp$, obtained by the vertical component of momentum $p_\perp(r_2) = 0$], and a starting point r_1. As in Refs. [14,45], by putting the effective incoming electron energy $E_\perp + I$ at a vertical component of projectile momentum, $p_\perp = 0$, one can obtain $r_1 = q_{eff}/(E_\perp + I)$. Here, $I = 0.754$ eV represents the binding energy of the loosely bounded affinity electron of the H^- projectile [10].

D. Population buildup

Owing to the small incident angle of a projectile with respect to the surface plane, the long trajectory path close to the surface leads to the projectile collision with a large number of surface lattice sites. To obtain the population probability of negative ions in the scattered beam after scattering from the MgO(100) surface, the probabilities of valence-band electron capture, electron loss to the conduction band, and the electron detachment into vacuum in a single binary collision with a surface O^{2-}_{as} should be calculated. The calculation results of these three electron-transfer probabilities are shown in Fig. 5. The integrated capture probability of $P_{cap}(Z, v) = \langle P_{cap}(R, v)\rangle_S$ and results of its projections on velocity v are displayed in Figs. 5(a) and 5(b), respectively. The probability of electron loss to the conduction band $P_{LS}(v)$ is shown in Fig. 5(c), and the electron-detachment probabilities of both $P^{q=-1.14}_{det}$ and $P^{q=-0.14}_{det}$ are shown in Fig. 5(d).

It is important to note that the electron detaches by a tunneling process in the interaction between H^- ions and different charged O anions [see Fig. 5(d)]. After a neutral hydrogen projectile captures an electron from the surface $O^{q_{eff}}_{as}$ with effective charge of $q_{eff} = -1.14$ [33], the Coulomb repulsive interaction between the formed H^- ion and this surface $O^{q'_{eff}}_{as}$ with a remaining effective charge of $q'_{eff} = -0.14$ will cause a tunneling detachment of the captured affinity electron of the H^- ion. Due to different Coulomb repulsive barriers, this tunneling detachment probability is obviously different from that in the interaction between H^- ions and other O^{2-}_{as} of the MgO(100) surface. Considering a neutral hydrogen atom is approaching the O^{2-}_{as} active site, it may capture an electron on the trajectory before the outer turning point (where the vertical component of effective electron momentum $p_\perp = 0$) to form a negative ion, which will subsequently interact with this O anion site with a remaining effective negative charge of $q'_{eff} = -0.14$. After the projectile captured an electron before the outer turning point, the subsequent interaction with this O anion site can of course be regarded as the negatively charged projectile colliding with this O anion site, and naturally the quantum tunneling detachment of the loosely bounded affinity electron of the negative ion should be taken into account. Moreover, as discussed above on the integration limits of Eq. (11), the outer turning point can greatly affect the tunneling probability. Thus, we make two approximations: (i) the electron tunneling detachment of the formed negative ion is negligible after the outer turning point in the entire interaction between a neutral projectile and an O^{2-}_{site}; (ii) the probability of the electron capture before the outer turning

point is the same as that after the outer turning point. These approximations are certainly quite crude but acceptable in our present treatment. Therefore, while a neutral hydrogen projectile collides with the O active anion site, the statistic factor of electron capture before the outer turning point is $\frac{1}{2}$, and the probability of negative-ion formation is $\frac{1}{2}P_{\rm cap}(1-P_{\rm det}^{q=-0.14})$ due to the electron detachment in the interaction between the formed negative ion and the O anion site with remaining effective negative charge. While the neutral projectile captures an electron after the outer turning point, which also has a statistic factor of $\frac{1}{2}$ for electron capture, the probability of negative-ion formation is $\frac{1}{2}P_{\rm cap}$. Thus, the probability of forming negative ions from the interaction between a neutral hydrogen atom and a surface $O_{\rm as}^{2-}$ is $P_{\rm cap}(1-\frac{1}{2}P_{\rm det}^{q=-0.14})$.

It can be seen that the present probability of electron capture is consistent with the results of other theoretical reports [11]. At low projectile energies, negative ions are destroyed dominantly by the interaction with surface Mg cations; that is, the affinity electrons of negative ions are lost via resonance charge transfer to the conduction band of the MgO crystal. Although the electron-detachment probability is close to 0 at low velocity, the resonance electron transfer from a H^- projectile to the conduction band near a surface Mg cation still makes the probability of negative-ion destruction close to 100%. However, the probabilities of the electron loss and detachment go into reverse at high velocity [see Figs. 5(c) and 5(d)]. This makes the negative-ion destruction easy in the entire energy range and the assumption of a constant destruction probability in Ref. [11] understandable. Additionally, the fact of the nearly same negative ion yields observed experimentally for H^- and H^0 incidence can be also explained by the negative-ion destruction probability presented here.

Considering a neutral projectile traveling in front of the MgO(100) surface, since there is no charge transfer with Mg cation sites, the electron transfer starts from a valence-band electron capture during a binary collision of the neutral projectile with a surface $O_{\rm as}^{2-}$. Upon the formation of a negative ion, electron transfer proceeds during subsequent collisions with other lattice sites along the scattering trajectory. Generally, electron capture of neutral projectiles and electron detachment of negative projectiles occur at the surface, $O_{\rm site}^{2-}$, and electron loss to the conduction band takes place at Mg cation sites. Similar to the method described in Ref. [46], the negative ion fraction $P(N)$ can be calculated by iteration of the collision number $N_{\rm coll}$ with the negative ion fraction of $n_{\rm min}$. One can easily get the negative ion fractions after the electron transfer by a single binary collision of a projectile with a Mg or O ionic site,

$$\begin{cases} n_{\rm min}^{\rm O} = (1-n_{\rm min})P_{\rm cap}\left(1-\frac{1}{2}P_{\rm det}^{q=-0.14}\right)+n_{\rm min}\left(1-P_{\rm det}^{q=-1.14}\right) \\ n_{\rm min}^{\rm Mg} = n_{\rm min}(1-P_{\rm LS}) \end{cases}. \tag{12}$$

Here, $n_{\rm min}$ is the negative ion fraction preceding the electron-transfer event and encountering the current Mg or O ionic site. $n_{\rm min}^{\rm O}$ and $n_{\rm min}^{\rm Mg}$ are the negative ion fractions after a binary collision of the projectile with O and Mg ionic sites, respectively. It should be noted here that $P_{\rm cap}$ in the $n_{\rm min}^{\rm O}$ expression is the result of $P_{\rm cap}(Z, v)$ averaged over the surface altitude range of $Z \in [2.5, 5]$ a.u. In the expression of negative ion fraction, $n_{\rm min}^{\rm O}$, the first term represents the probability of the negative-ion conversion of the neutral projectiles at the active O anion site. It includes both probabilities of the valence-band electron capture from the active O anion site, $P_{\rm cap}$, and the detachment of the affinity electron of the formed negative ion at the same anion site with a remain charge of $q=-0.14$, $P_{\rm det}^{q=-0.14}$. The second term in the $n_{\rm min}^{\rm O}$ expression represents the incident H^- projectiles without electron detachment during the interaction with the active O anion site, where $P_{\rm det}^{q=-1.14}$ represents the probability of electron detachment while a H^- encounters an active O anion with an effective charge of $q=-1.14$ [33]. The term $P_{\rm LS}$ in the $n_{\rm min}^{\rm Mg}$ expression represents the probability of electron loss to the conduction band of the MgO crystal for H^- projectiles.

Considering the statistical results of multiple collisions of a projectile with a large number of Mg and O sites along its trajectory, one can obtain the average negative ion fraction $\langle n_{\rm min}\rangle$ after a projectile encounters the lattice site twice (one O site and one Mg site),

$$\begin{aligned} \langle n_{\rm min}\rangle =& n'_{\rm min}(1-P_{\rm LS})\left(1-P_{\rm det}^{q=-1.14}\right) \\ &+ P_{\rm cap}\left(1-\tfrac{1}{2}P_{\rm det}^{q=-0.14}\right)\left[\left(1-\tfrac{1}{2}P_{\rm LS}\right)\right. \\ &\left.- n'_{\rm min}(1-P_{\rm LS})\right]. \end{aligned} \tag{13}$$

Here, $n'_{\rm min}$ in Eq. (13) is the negative ion fraction preceding electron transfer before the collision with the current two lattice sites. The collision number $N_{\rm coll}$ is determined by $N_{\rm coll} \approx 2d/(a\tan\alpha)$, where a is the lattice constant; d represents the surface altitude range within which the trajectories contribute most to electron transfer [16] and can be estimated by the results in Ref. [11].

The calculation results (red solid line) of negation-ion production and the available experimental data for H^0 (squares) and H^- (circles) incidence from Ref. [9] are shown in Fig. 6(a). It is observed that our present result which employed $\beta = 0.2$ for the affinity electron of H^- ion loss to the conduction band of MgO fits the experimental data well in the whole energy range. The minor difference of 0.01% between the results of H^- and H^0 projectiles gives nearly the same negative ion yields. For further details of the effect of the value of the β parameter to the final negative ion fractions, the results of negative ion fractions of $\beta = 0.1$ (blue dashed-dotted line) and 0.3 (green dashed-dot-dotted line) are also shown in Fig. 6(a), respectively. Compared with experimental results, the β values taken from the range of $\beta \in [0.1, 0.3]$ are all actually acceptable within the experimental uncertainty. The H^- ion fractions increase with projectile energy E and reach saturation above about $E = 1.5$ keV. As discussed above, combining the electron loss to the conduction band of the MgO crystal with the quantum tunneling detachment of the loosely bounded affinity electron of H^- ions, the probability of negative-ion destruction is approximately constant in the entire projectile energy range; that is, it does not follow the projectile energy. Therefore, the final behavior of H^- ion fractions is consistent with that of electron-capture probability [see Fig. 5(b)]. Figure 6(b) displays the behavior of negative ion yields for the neutral and negative hydrogen projectiles scattering from the MgO(100) surface in the absence of

quantum tunneling detachment and resonant electron loss to the conduction band, respectively. When the resonant electron loss is absent, the negative ion yield for H^- incidence is higher than that for H^0 incidence in the low-energy region of $E \leqslant 0.7\,\text{keV}$ ($v \leqslant 0.17\,\text{a.u.}$), due to the small tunneling detachment probabilities; for the energy region of $E \geqslant 0.7\,\text{keV}$, the negative ion yield for H^- incidence is the same as that for H^0 incidence. In the absence of tunneling detachment, the negative ion yields for the two projectiles' (H^- and H^0) incidence are indistinguishable from each other in the low-energy region of $E \leqslant 1.2\,\text{keV}$ ($v \leqslant 0.22\,\text{a.u.}$). It indicates the large enough probability of resonant electron loss for the destruction of negative ions. There is a small gap between the two yields when the incident energies approach $E = 6\,\text{keV}$ ($v = 0.5\,\text{a.u.}$), because of the decreasing probability of resonant electron loss. The negative-ion destruction is dominated by the resonant electron loss at incident energies of $E \leqslant 0.7\,\text{keV}$ ($v \leqslant 0.17\,\text{a.u.}$), while quantum tunneling detachment becomes efficient at energies of of $E \geqslant 1.2\,\text{keV}$ ($v \geqslant 0.22\,\text{a.u.}$). Here, also the negative ion yield for neutral atoms' incidence without any destruction channels is shown in Fig. 6(b) for comparison.

The employed surface altitude range of $Z \in [2.5, 5.0]$ a.u. has been proved to be the main surface altitude range for charge exchange [14,15,47]. In addition, the closest approach to the surface in Ref. [11] indicates that this surface altitude range can be reached by projectiles with energies studied in our present work. It should be noted here that the neglect of the electron-capture contributions to the final negative ion yields at $Z > 5$ a.u. is due to the large energy defect and small coupling strength of the electron-capture reaction. In the high-energy region, the projectile turning point is very close to the surface ($Z < 2.5$ a.u.). However, the projectiles will go away from the surface and reach an altitude of $Z > 2.5$ a.u. when leaving the turning point. Due to the high efficiency of charge exchange, the final fraction is still consistent with the experimental data. In the case of F^0/F^- incidence, similar to the case of H^0/H^- incidence without including the resonant electron loss, the electron transfer from the projectiles to the conduction band is suppressed and negative ions are destroyed only via the quantum tunneling detachment. Therefore, owing to a very efficient electron loss by the resonant electron transfer to the conduction band in the low-energy region, the H^- fraction in the low-energy region shows a completely different behavior from the F^- fraction.

V. CONCLUSIONS

We present a simple theoretical description of negative ion formation by grazing scattering of H^0 and H^- projectiles from the MgO(100) surface. A sub-eV order of calculated energy defect between the affinity level of H^- ions and the conduction band of MgO crystal reveals a picture of electron loss to the conduction band by a nearly resonant electron transfer participating in the negative-ion destruction. For quantum tunneling detachment, in addition to the encounter of H^- projectiles with O anion active sites, the tunneling detachment caused by the remaining charge of $q = -0.14$ left at $O_{\text{site}}^{q_{\text{eff}}=-1.14}$ after a valence-band electron captured by a neutral projectile is also revealed. Hence the negative-ion destruction mainly involves two processes: (1) resonant electron transfer from the affinity level of a negative projectile to the conduction band, and (2) the Coulomb repulsive barrier tunneled to the vacuum level of the affinity electron of a H^- ion in the interaction with surface anion sites. Combining the valence-band electron capture with the two negative-ion destruction channels presented here, the final negative ion yield was calculated and is consistent with the available experimental results in the entire velocity range. By comparing the experiment measurement with the calculated results with or without including the negative-ion destruction channels discussed above, one can find that the negative-ion destruction is dominated by the resonant electron loss to the conduction band in the low-energy region of $E \leqslant 0.7\,\text{keV}$ ($v \leqslant 0.17\,\text{a.u.}$), whereas quantum tunneling detachment to vacuum becomes efficient in the high-energy region of $E \geqslant 1.2\,\text{keV}$ ($v \geqslant 0.22\,\text{a.u.}$).

It should be noted that the parameter β depending on the coupling strength of the resonant electron-transfer process is given as a constant in our present model. To accurately calculate it, a complete quantum chemistry calculation beyond the main scope of our present work is required. A more detailed investigation and further development are needed in order to describe in more depth the electron transfer on insulating oxide surfaces.

ACKNOWLEDGMENT

This work was financially supported by the Youth Foundation of Lanzhou City University (Grant No. LZCU-QN2020-02).

[1] V. E. Henrich and P. A. Cox, *The Surface Science of Metal Oxides* (Cambridge University Press, New York, 1996).
[2] G. Somorjai, *Chemistry in two Dimensions: Surfaces* (Cornell University Press, Ithaca, NY, 1981).
[3] A. Silverman, J. Adler, and R. Kalish, Phys. Rev. B **83**, 224206 (2011).
[4] U. K. Chaturvedi, V. Shrinet, and A. K. Nigam, Phys. Rev. B **33**, 5834 (1986).
[5] C. Auth, T. Hecht, T. Igel, and H. Winter, Phys. Rev. Lett. **74**, 5244 (1995).
[6] H. Winter, Phys. Rev. A **46**, R13 (1992).
[7] J. E. Miraglia, Phys. Rev. A **90**, 062715 (2014).
[8] H. Winter, Prog. Surf. Sci. **63**, 177 (2000); Phys. Rep. **367**, 387 (2002).
[9] S. Ustaze, R. Verucchi, S. Lacombe, L. Guillemot, and V. A. Esaulov, Phys. Rev. Lett. **79**, 3526 (1997).
[10] S. A. Deutscher, A. G. Borisov, and V. Sidis, Phys. Rev. A **59**, 4446 (1999).
[11] S. A. Deutscher, A. G. Borisov, and V. Sidis, Nucl. Instrum. Methods Phys. Res., Sect. B **157**, 61 (1999).
[12] A. G. Borisov and V. A. Esaulov, J. Phys.: Condens. Matter **12**, R177 (2000).

[13] H. Zhou, L. Chen, D. Feng, Y. Guo, M. Ji, G. Wang, W. Zhou, Y. Li, L. Zhao, and X. Chen, Phys. Rev. A **85**, 014901 (2012).
[14] H. Zhou, W. Zhou, M. Zhang, L. Zhou, Y. Ma, G. Wang, Y. Wu, B. Li, and X. Chen, Phys. Rev. A **93**, 062708 (2016); W. Zhou, H. Zhou, M. Zhang, L. Zhou, Y. Li, B. Li, and X. Chen, *ibid.* **94**, 052708 (2016).
[15] A. G. Borisov and V. Sidis, Phys. Rev. B **56**, 10628 (1997).
[16] A. G. Borisov, V. Sidis, and H. Winter, Phys. Rev. Lett. **77**, 1893 (1996).
[17] B. Jin, H. Zhou, Z. Zong, X. Zhang, G. Wang, L. Zhoua, and X. Chen, RSC Adv. **11**, 4489 (2021).
[18] F. W. Meyer, E. Galutschek, and M. Hotchkis, in *Applications of Accelerators in Research and Industry: Twentieth International Conference*, AIP Conf. Proc. No. 1099 (AIP, Melville, NY, 2009), p. 308.
[19] L Gao, W. Gan, G. Cao, X. Zhanc, T. Qianga, and J. Li, Appl. Surf. Sci. **425**, 889 (2017).
[20] R. L. Tang, R. Si, Z. J. Fei, X. X. Fu, Y. Z. Lu, T. Brage, H. T. Liu, C. Y. Chen, and C. G. Ning, Phys. Rev. Lett. **123**, 203002 (2019).
[21] G. Cerchiari, A. Kellerbauer, M. S. Safronova, U. I. Safronova, and P. Yzombard, Phys. Rev. Lett. **120**, 133205 (2018).
[22] P. Yzombard, M. Hamamda, S. Gerber, M. Doser, and D. Comparat, Phys. Rev. Lett. **114**, 213001 (2015).
[23] J. Shaw, D. Monismith, Y. Zhang, D. Doerr, and H. S. Chakraborty, Phys. Rev. A **98**, 052705 (2018).
[24] T. J. Millar, C. Walsh, and T. A. Field, Chem. Rev. **117**, 1765 (2017).
[25] G. Cartry, D. Kogut, K. Achkasov, J. Layet, T. Farley, A. Gicquel, J. Achard, O. Brinza, T. Bieber, H. Khemliche, P. Roncin, and A. Simonin, New J. Phys. **19**, 025010 (2017).
[26] J. E. Mayer and M. M. Maltbie, Z. Phys. **75**, 748 (1932).
[27] J. B. Zhou, H. C. Lou, T. Gustafsson, and P. Häberle, Surf. Sci. **302**, 350 (1994).
[28] D. M. Roessler and W. C. Walker, Phys. Rev. **159**, 733 (1967); J. Opt. Soc. Am. **57**, 835 (1967).
[29] L. H. Tjeng, A. R. Vos, and G. A. Sawatzky, Surf. Sci. **235**, 269 (1990).
[30] N. F. Mott and M. J. Littleton, Trans. Faraday Soc. **34**, 485 (1938); W. B. Fowler, Phys. Rev. **151**, 657 (1966); G. D. Mahan, Phys. Rev. B **21**, 4791 (1980).
[31] G. Pacchioni and T. Minerva, Surf. Sci. **275**, 450 (1992).
[32] K. M. Neyman and N. Rösch, Chem. Phys. **168**, 267 (1992).
[33] S. Russo and C. Noguera, Surf. Sci. **262**, 245 (1992).
[34] J. Goniakowski, S. Bouette-Russo, and C. Noguera, Surf. Sci. **284**, 315 (1993).
[35] M. A. Nygren and L. G. M. Pettersson, J. Chem. Phys. **105**, 9339 (1996).
[36] Y. Nakajima and D. J. Doren, J. Chem. Phys. **105**, 7753 (1996).
[37] Z. Zong, H. Zhou, B. Jin, X. Zhang, G. Wang, L. Zhou, and X. Chen, J. Phys. Chem. C **124**, 18054 (2020).
[38] A. G. Borisov, J. P. Gauyacq, V. Sidis, and A. K. Kazansky, Phys. Rev. B **63**, 045407 (2001).
[39] P. M. Echenique and A. Howie, Ultramicroscopy **16**, 269 (1985); N. R. Arista, Phys. Rev. A **49**, 1885 (1994).
[40] J. R. Tessman, A. H. Kahn, and W. Shockley, Phys. Rev. **92**, 890 (1953).
[41] E. D. Palik and W. R. Hunter, *Handbook of Optical Constants of Solids* (Academic Press, New York, 1985).
[42] Y. N. Demkov, Sov. Phys. JETP **18**, 138 (1964).
[43] A. G. Borisov, D. Teillet-Billy, J. P. Gauyacq, J. A. M. C. Silva, A. Mertens, C. Auth, and H. Winter, Phys. Rev. B **59**, 8218 (1999).
[44] A. G. Borisov and J. P. Gauyacq, Phys. Rev. B **62**, 4265 (2000).
[45] J. M. Rost, Phys. Rev. Lett. **82**, 1652 (1999).
[46] H. Winter, A. Mertens, S. Lederer, C. Auth, F. Aumayr, and H. P. Winter, Nucl. Instrum. Methods Phys. Res., Sect. B **212**, 45 (2003).
[47] C. Auth, A. Mertens, H. Winter, A. G. Borisov, and V. Sidis, Phys. Rev. A **57**, 351 (1998).